Thermal Response of Graphite Epoxy Composites Subjected to Rapid Heating

C.A. GRIFFIS, R.A. MASUMURA, AND C.I. CHANG

Material Science and Technology Division

March 31, 1981

NAVAL RESEARCH LABORATORY
Washington, D.C.

SECURITY CLASSIFICATION OF THIS PAGE (When Data Entered)

(9) **REPORT DOCUMENTATION PAGE**

READ INSTRUCTIONS BEFORE COMPLETING FORM

1. REPORT NUMBER	2. GOVT ACCESSION NO.	3. RECIPIENT'S CATALOG NUMBER
NRL Memorandum Report 4479	AD-A096	398

4. TITLE (and Subtitle)

(6) THERMAL RESPONSE OF GRAPHITE EPOXY COMPOSITE SUBJECTED TO RAPID HEATING

5. TYPE OF REPORT & PERIOD COVERED
Interim Report on a continuing NRL problem.

6. PERFORMING ORG. REPORT NUMBER

7. AUTHOR(s)

(10) C. A. Griffis, R. A. Masumura, and C. I. Chang

8. CONTRACT OR GRANT NUMBER(s)
(16) F62544

9. PERFORMING ORGANIZATION NAME AND ADDRESS
Naval Research Laboratory
Washington, D.C. 20375
(11) 31 Mar 81

10. PROGRAM ELEMENT, PROJECT, TASK AREA & WORK UNIT NUMBERS
(17) 62761, ZF61544007, 0300-A

11. CONTROLLING OFFICE NAME AND ADDRESS
Naval Air Systems Command
Washington, D.C. 20360

12. REPORT DATE
March 31, 1981

13. NUMBER OF PAGES
(12) 23 22

14. MONITORING AGENCY NAME & ADDRESS (if different from Controlling Office)
(14) NRL-MR-4479

15. SECURITY CLASS. (of this report)
UNCLASSIFIED

15a. DECLASSIFICATION/DOWNGRADING SCHEDULE

16. DISTRIBUTION STATEMENT (of this Report)

Approved for public release; distribution unlimited.

17. DISTRIBUTION STATEMENT (of the abstract entered in Block 20, if different from Report)

18. SUPPLEMENTARY NOTES

19. KEY WORDS (Continue on reverse side if necessary and identify by block number)

Heat transfer	Convection
Fiber-reinforced composites	Laser irradiation
Finite difference methods	Ablation
Radiation	Surface recession rate
Conduction	Embedded thermocouples

20. ABSTRACT (Continue on reverse side if necessary and identify by block number)

A one-dimensional finite difference analysis describing the transient thermal response of fiber-reinforced organic matrix composite plates subjected to intense surface heating is presented. The effects of fiber ablation, matrix decomposition, and radiation and convective heat losses are included in the formulation. Numerical results are in good agreement with mass loss and thermocouple measurements obtained from laser irradiation tests on AS/3501-6 graphite epoxy coupons. A steady state analytic solution is also given which provides a reasonable estimate of the surface recession rate over much of the surface irradiation period.

DD FORM 1 JAN 73 1473 EDITION OF 1 NOV 65 IS OBSOLETE
S/N 0102-LF-014-6601

232950

SECURITY CLASSIFICATION OF THIS PAGE (When Data Entered)

CONTENTS

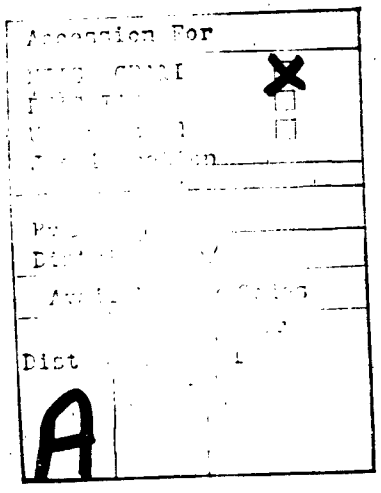

THERMAL RESPONSE OF GRAPHITE EPOXY COMPOSITE SUBJECTED TO RAPID HEATING

1. INTRODUCTION

Due to their high strength to weight ratio at low temperatures, fiber reinforced organic matrix composites have been successfully utilized in numerous military and space applications. However, intense heating produced by fire or laser or irradiation can adversely effect the integrity of composite structures due to the rapid degradation of mechanical properties (tensile and shear strength, elastic moduli, etc.) at temperatures above 200°C (1). Severe thermal irradiation may also induce undesirable geometric changes through ablation of critical load carrying members or by generation of high stress concentration due to localized burnthrough (2). Thus, accurate modeling of thermal response constitutes an important element in assessing the overall reliability of composite structures subjected to rapid, high-intensity heating.

In the present study, a simplified one-dimensional mathematical approach is presented for transient heat transfer analysis of composite plates exposed to surface heating. This model is then employed, in conjunction with an experimental study, to verify recently proposed (3) thermophysical properties of AS/3501-6 graphite epoxy laminate. In a separate investigation, computational results (temperature distributions and ablative characteristics) from the thermal analysis will be coupled with detailed stress analyses to evolve a thermomechanical failure criterion for AS/3501-6 laminates under combined laser irradiation and uniaxial tensile loading.

2. ANALYTICAL DEVELOPMENT

2.1 Heat Transfer Equations for One-Dimensional Model

Since the current study is concerned largely with scenerios where a uniform high-intensity energy flux is applied over an area whose characteristic dimensions are significantly greater than the composite

Manuscript submitted January 12, 1981

thickness, a one-dimensional approach is adopted. Heat transfer is assumed to occur by conduction in the thickness direction, i.e., normal to the plane of the fibers. Thermal decomposition of the organic matrix material (e.g., epoxy resin) is approximated (3) by elevation of the bulk heat capacity over an appropriate temperature range; thus, temperature dependent material properties are included in the treatment. In addition, the fiber reinforcing component (e.g., graphite or boron) as well as any residual matrix constituents are assumed to undergo a simple sublimation reaction when the surface temperature reaches a predetermined constant value. Mathematically this surface ablation may be considered equivalent to a classical melting problem (4) in which the melt is instantaneously removed. For subsequent numerical convenience, a convective coordinate system (5,6) is adopted which moves continuously with the ablating fibers as indicated in Fig.1, i.e.,

$$z = x - x_b, \tag{1}$$

where z and x are the convected and global coordinates, respectively, and $x_b(t)$ denotes the instantaneous position of the receding surface. With respect to the moving coordinate, the one-dimensional Fourier conduction equation is given by

$$\frac{\partial}{\partial z}\left[k\frac{\partial T}{\partial z}\right] + \rho C_p V\frac{\partial T}{\partial z} = \rho C_p\frac{\partial T}{\partial t}, \tag{2}$$

where $T(z,t)$, k,ρ and C_p represent the temperature, thermal conductivity, density, and heat capacity, respectively. The quantity $V \equiv dx_b/dt$ denotes the surface recession rate and is regarded as an unknown function of time.

Subsequent to the onset of abiation ($t < t_0$), boundary conditions at the irradiated surface ($z = 0$) include:

$$T(0,t) = T_s = \text{constant} \tag{3}$$

and a straightforward energy balance expressed by

$$\rho H_s V = \alpha I_0 + k\frac{\partial T}{\partial z} + I_r + I_c, \tag{4}$$

in which H_s is an effective heat of ablation (assumed constant) and I_0 represents the incident heat flux. Surface energy losses due to radiation and convection are I_r and I_c, respectively, in Eq. (4), and the coupling coefficient α denotes the fraction of the incident energy which is absorbed by the receiver.

The radiation loss cited above is computed according to

$$I_r = \sigma \epsilon \ (T_0^4 - T_s^4), \tag{5}$$

where σ is the Stefan-Boltzmann constant; ϵ is the surface emissivity; and T_0 represents the surrounding air temperature.

The convective heat loss, I_c, resulting from the flow of high velocity air parallel to the irradiated surface is given by the Newton heat transfer equation, viz.,

$$I_c = h(T_r - T_s), \tag{6}$$

where h and T_r are the convection coefficient and air recovery temperature, respectively. In the present study a laminar boundary layer is considered in which case the Pohlhaussen flat plate equation may be used to estimate the convection coefficient. A simplified form (7) of this equation is:

$$h\,(btu/in^2 - sec - {}^\circ F) = 0.3\frac{k_a}{s}\,\mathrm{Re}^{1/2}, \tag{7}$$

where k_a is the thermal conductivity of air; s represents the distance from the leading edge of the boundary layer; and Re is the Reynolds Number.*

Due to the low transverse conductivity exhibited by many organic matrix composites at elevated temperatures, a relatively small temperature rise is frequently observed at the unirradiated surface over the exposure times of interest. Consequently the rear surface is assumed to be insulated, i.e.,

$$\frac{\partial T}{\partial z} = 0 \text{ at } z = l - x_b, \tag{8}$$

where l is the initial laminate thickness.

It may be noted that prior to ablation ($t < t_0$, $T(0,t) < T_s$), Eqs. (1) and (2) are applicable with $x_b = V = 0$. Appropriate boundary conditions are then expressed by Eqs.(3-8) with $V = 0$ and the surface temperature T_s regarded as an unknown function of time.

* The semi-empirical expressions given in Ref. (7) were utilized to evaluate the dependence of k_a and Re on surface temperature. Also, the thermodynamic analysis in Ref. (7) was employed to compute T_r (Eq. (6)) in terms of the airstream velocity and T_0; this approach assumes a constant value of the recovery factor equal to 0.88.

2.2 Numerical Solution

Solutions to the nonlinear boundary value problem defined by Eqs. (1-8) were obtained numerically using a modified Crank-Nicholson finite difference method. Figure 1 gives a schematic representation of the one-dimensional array of nodal points employed in the calculations. To efficiently characterize the steep temperature gradient near the irradiated surface, a variable mesh spacing is used in which the the nodal separation increases with increasing distance from the front surface. Since Eqs. (1-8) are written with respect to the convected coordinate z, the entire finite difference grid is uniformly translated along with the receding front surface as the solution proceeds. However, because the global coordinate of the unirradiated surface ($x = l$) is fixed, the total number of nodes actually utilized decreases as ablation continues; i.e., once a node has traversed the rear surface it is ignored in subsequent calculations.

With respect to the generic sequence of interior nodal points $i - 1$, i, $i + 1$ (Fig. 1), finite difference approximations for the first and second temperature derivatives at node i are:

$$\left.\frac{\partial T}{\partial z}\right|_{i,j} = \frac{T_{i+1,j} + (r^2 - 1)T_{i,j} - r^2 T_{i-1,j}}{r(r+1)(z_i - z_{i-1})} \tag{9a}$$

and

$$\left.\frac{\partial^2 T}{\partial z^2}\right|_{i,j} = \frac{2[rT_{i-1,j} + T_{i+1,j} - (r+1)T_{i,j}]}{r(r+1)(z_i - z_{i-1})^2}, \tag{9b}$$

where $r \equiv (z_{i+1} - z_i)/(z_i - z_{i-1})$ and the subscripts i and j on T and its derivatives indicate evaluation at coordinate z_i at time t_j. As described in Ref. (8) the Crank-Nicholson method entails using in Eqs. (1-8) the following average spatial derivatives over a generic time increment $\Delta t \equiv t_{j+1} - t_j$.

$$\left.\frac{\partial T}{\partial z}\right|_{i,m} = \left[\left.\frac{\partial T}{\partial z}\right|_{i,j+1} + \left.\frac{\partial T}{\partial z}\right|_{i,j}\right]/2 \tag{10a}$$

and

$$\left.\frac{\partial^2 T}{\partial z^2}\right|_{i,m} = \left[\left.\frac{\partial^2 T}{\partial z^2}\right|_{i,j+1} + \left.\frac{\partial^2 T}{\partial z^2}\right|_{i,j}\right]/2, \tag{10b}$$

where the subscript m implies evaluation at the mean time over the increment $t_m = (t_{j+1} + t_j)/2$. The corresponding average time derivative over the interval Δt is represented by the forward difference expression:

$$\left.\frac{\partial T}{\partial t}\right|_{i,m} = \frac{T_{i,j+1} - T_{i,j}}{\Delta t}. \tag{11}$$

Substitution of Eqs. (9), (10), and (11) into Eq. (2) yields the general difference equation to be satisfied at all nodal points, viz.,

$$\left[\frac{-\lambda_1 + \lambda_2 r}{r+1}\right] T_{i-1,j+1} + \left[1 - \lambda_2\left[\frac{r-1}{r}\right] + \frac{\lambda_1}{r}\right] T_{i,j+1} - \left[\frac{\lambda_1 + \lambda_2}{r(r+1)}\right] T_{i+1,j+1} =$$
$$\left[\frac{\lambda_1 - \lambda_2 r}{r+1}\right] T_{i-1,j} + \left[1 + \lambda_2\left[\frac{r-1}{r}\right] - \frac{\lambda_1}{r}\right] T_{i,j} + \left[\frac{\lambda_1 + \lambda_2}{r(r+1)}\right] T_{i+1,j} +$$
$$\lambda_3\Big[\; T_{i+1,j+1} + T_{i+1,j} + (r^2 - 1)(T_{i,j+1} + T_{i,j}) - r^2(T_{i-1,j+1} + T_{i-1,j})\Big]^2. \tag{12}$$

where

$$\lambda_1 = \frac{k\,\Delta t}{\rho C_p (z_i - z_{i-1})^2},$$
$$\lambda_2 = \frac{V_m \Delta t}{2(z_i - z_{i-1})},$$
$$\lambda_3 = \frac{(dk/dT)\,\Delta t}{4r^2(1+r)^2(z_i - z_{i-1})^2 \rho C_p}.$$

The material properties $(\rho, C_p, k, dk/dT)$ referred to in Eq. (12) are generally temperature dependent and are to be evaluated at the mean temperature $T_{i,m}$ existing at node i over the time Δt. Similarly, the surface recession rate V_m appearing in λ_2 is an average value associated with time t_m.

According to Eq. (3) one boundary condition at the irradiated surface (node 1 in Fig. 1) is simply the constant temperature condition

$$T(0,t_j) \equiv T_{1,j} = T_s, \tag{13}$$

which is valid for $t > t_0$. The conservation of energy condition, Eq. (4), is also applicable at node 1 and may be conveniently expressed in difference form by introduction of a virtual node at $z = -z_2$ as indicated in Fig. 1. A straightforward substitution of Eqs. (9a) and (10a) into Eq. (4) then gives

$$T_{2,j+1} + T_{2,j} - T_{0,j+1} - T_{0,j} = \frac{-4z_2}{k}(Q - \rho H_s V_m) \tag{14}$$

in which $Q \equiv \alpha I_0 + I_r + I_c$ is constant by virtue of Eq. (3) providing I_0 does not vary with time. By applying the general expression, Eq. (12), at node 1 and combining the result with Eq. (14), the virtual temperatures ($T_{0,j+1}$ and $T_{0,j}$) are eliminated. This gives

$$2T_s - T_{2,j+1} - T_{2,j} = \left[\frac{\rho H_s V_m - Q}{k}\right]\left[\frac{\rho C_p z_1^2 V_m}{k} - 2z_2 + \frac{(dk/dT)\, z_1^2}{k^2}\right] \tag{15}$$

where all material properties are evaluated at the surface temperatue T_s.

The zero heat flux condition at the unirradiated surface is implemented numerically by again using a virtual node at $z = 2z_r - z_{r-1}$ (see Fig. 1). A simple two-term series expansion about node r is employed to estimate the temperature gradient at the insulated surface, viz.,

$$\left.\frac{\partial T}{\partial z}\right|_{surf.,m} = \left.\frac{\partial T}{\partial z}\right|_{r,m} + \left.\frac{\partial^2 T}{\partial z^2}\right|_{r,m} \delta_m = 0, \tag{16}$$

where the second equality follows from Eq. (8), and δ_m refers to the temporally averaged distance between node r and the unirradiated surface over the time increment Δt. The quantity δ_m can be expressed by the recursive relation:

$$\delta_m = \frac{\delta_{j+1} + \delta_j}{2} = \delta_j - \frac{V_m \Delta t}{2}, \tag{17}$$

in which δ_j is the separation existing at the begining of the time increment, i.e., at $t = t_j$. Combination of Eqs. (9), (10), (16), and (17) yields:

$$2(T_{r,j+1} + T_{r,j})\lambda_4 - (T_{r-1,j+1} + T_{r-1,j})(\lambda_4 - 1/2) = (T_{r+1,j+1} + T_{r+1,j})(\lambda_4 + 1/2), \tag{18}$$

where

$$\lambda_4 = \frac{2\delta_j - V_m \Delta t}{2(z_r - z_{r-1})}.$$

Finally the temperatures $T_{r+1,j+1}$ and $T_{r+1,j}$ at the virtual node can be eliminated by invoking the general difference relationship (Eq. (12)) at node r and combining the result with Eq. (18). This procedure provides:

$$\left[-\lambda_1 + \lambda_2 + \frac{(\lambda_1 + \lambda_2)(2\lambda_4 - 1)}{2\lambda_4 + 1}\right] T_{r-1,j+1} + \left[2(1 + \lambda_1) - \frac{4\lambda_4(\lambda_1 + \lambda_2)}{2\lambda_4 + 1}\right] T_{r,j+1} =$$
$$\left[\lambda_1 - \lambda_2 - \frac{(\lambda_1 + \lambda_2)(2\lambda_4 - 1)}{2\lambda_4 + 1}\right] T_{r-1,j} + \left[2(1 - \lambda_1) + \frac{4\lambda_4(\lambda_1 + \lambda_2)}{2\lambda_4 + 1}\right] T_{r,j} +$$
$$\left[\frac{32\lambda_3\lambda_4^2}{(2\lambda_4 + 1)^2}\right](T_{r,j+1} + T_{r,j} - T_{r-1,j+1} - T_{r-1,j})^2. \tag{19}$$

Equations (12), (15) and (19) define an implicit numerical method for solution to the present boundary value problem; given the solution at a generic time t_j, simultaneous solution of these equations provides the temperature distribution and recession rate at t_{j+1}. Since the difference equations are obviously nonlinear, their solution at each time step was obtained iteratively using the method of successive approximations. For a typical time increment $\Delta t = t_{j+1} - t_j$, the following algorithm was adopted. In the first iteration, the quadratic terms appearing in Eqs. (12) and (19) as well as the values of $\lambda_1, \lambda_2, \lambda_3$, and λ_4 were evaluated using the known nodal temperatures and recession rate existing at t_j. The resulting linear versions of Eqs. (12) and (19) were solved simultaneously for the temperatures of nodes 2 through r at t_{j+1}. Then, using Eq. (15) in conjunction with the recently computed $T_{2,j+1}$, an initial estimate of V_m was calculated. The process was then repeated using the most recent temperatures and V_m to generate a new (updated) linear form of Eqns. (12) and (19). At each time step, the calculations were continued until uniform values of V_m (within two percent) were obtained in successive iterations.

As suggested in Sec. 2.1 finite difference expressions analogous to Eqs. (12), (15), and (19) may be developed for pre-ablation regime ($t < t_0$) by noting that the surface temperature $T_{1,j}$ is variable and that $V_m = 0$. The resulting simultaneous difference equations are again nonlinear necessitating use of an iterative procedure. A method similar to that described above was employed in which convergence was based on constancy of surface temperature (rather than V_m) in successive iterations.

EXPERIMENTAL PROCEDURE AND MATERIAL PROPERTIES

3.1 Laser Irradiation Tests

To evaluate the analytical model, laminated composite panels were subjected to rapid heating using the 15 kw, continuous wave, CO_2 laser at NRL. Twenty-ply AS/3501-6 graphite epoxy coupons having in-plane dimensions 5.6 × 10 cm. were fabricated by the NRL Chemistry Division. The panel thickness was 2.54 mm. and the ply layup sequence was

$$\left[+45, -45, 90, 0, 0, 0, -45, +45, 0, 0,\right]_s,$$

where the subscript denotes symmetry about the laminate midthickness and 0, + 45, − 45, etc. indicate the angular orientation of the lamina fibers with respect to the lengthwise direction of the specimen. To measure the thermal response during irradiation, one thermocouple was embedded in the 11th ply during specimen fabrication and a second was placed on the rear surface (ply 20). In addition, an optical pyrometer was employed to establish the front surface temperature. Testing was conducted at several intensity levels (I_0) which were generated using a fixed 25mm beam diameter with variable power output. To simulate aerodynamic cooling effects, a Mach 0.3 airflow was applied parallel to the irradiated surface during each test.*

3.2 Thermophysical Properties

The temperature dependence of the material properties of AS/3501-6 which were employed in the numerical calculations are indicated in Fig. 2. These properties were obtained from Ref. (3) with minor modifications. The density variation $\rho(T)$ proposed in Ref. (3) was increased uniformly by 6 percent based on a higher room temperature value observed for the composite used in the present experiments. The plateau in the heat capacity curve $C_p(T)$ for $343 < T < 510°C$ represents additional heat absorbed during resin (matrix) decomposition; effective heat capacity values over this range were computed (3) using a theoretically derived latent heat of 996 J per gram of resin. In the present work the abrupt variations in C_p at 343 and 510°C suggested in Ref. (3) were replaced by more gradual changes occurring over 28°C intervals. Similarly, a smooth variation in conductivity $k(T)$ and a less severe 28°C transition in in $\rho(T)$ were introduced at 538°C. These modest shape changes in the property curves produced no significant change in analytical results and were adopted soley to provide enhanced stability and convergence characteristics in the numerical calculations.

As noted in the $C_p(T)$ curve of Fig. 2, the values of H_s and T_s for graphite sublimation were assumed to be 43 kJ/g and 3316°C, respectively. These properties were also obtained from Ref. (3).

* For these experiments the appropriate value of s to be used in the computation of the convection coefficient, Eq. (7), is 10.48 cm.

4. DISCUSSION OF RESULTS

The accuracy of the analytical procedure and assumed material properties may be assessed by comparison of the experimental and numerical results shown is Figs. 3, 4, and 5 for incident beam intensities (I_0) of 0.232, 1.33, and 2.79 kw/cm^2, respectively.* It is noted that the calculated and measured temperatures agree reasonably well, particularly at the lowest intensity level (Fig. 3) where the disparity is less than 45°C over most of the exposure time investigated. Examination of the numerical results for the 2.79 kw/cm^2 case, Fig. 5, reveals that the rapid increase in interior (ply 11) temperature after approximately 4 seconds is due to the close proximity of the advancing irradiated surface to the (global) $x = 1.4$ mm coordinate. The comparable increase in the embedded thermocouple response suggests that the ablation characteristics of the laminate are modeled quite well.

Figures 3-5 also indicate good correspondence between predicted and measured front surface temperatures. The lower temperature, 1860°C, measured after irradiation for 9.2 sec at 0.232 kw/cm^2 is reasonably close to the corresponding analytical result of 2132°C. No ablation is predicted for this test condition. On the other hand, significant ablation is projected for the 1.33 and 2.79 kw/cm^2 beam intensities and the measured surface temperatures, viz. 2938 and 3371°C, respectively, compare very well with the assumed 3316°C temperature level necessary to sustain graphite sublimation.

Figure 6 compares the analytical and experimental mass loss as a function of exposure time for material subjected to an *average* intensity of 1.81 kw/cm^2. The analytical $\Delta m(t)$ was determined from the easily derived expression

$$\Delta m(t) = A \int_{x_b(t)}^{l} [\rho_0 - \rho(T)]dx,$$

where $\rho(T)$ is given in Fig. 2; ρ_0 represents the initial (room temperature) density; and A is the total beam area. The temperature distribution $T = T(x,t)$ as well as the instantaneous position of the irradiated surface $x_b(t)$ were obtained from the numerical solution. Although excellent agreement between

* These intensities refer to maximum values existing at the center of the beam. Also, the surface emissivity (ϵ) and absorption coefficient (α) were both assigned a value of 0.92 in the numerical calculations.

predicted and measured mass loss is evident, it should be noted that an average rather than peak intensity was employed in the computation of $T(x,t)$ and x_b. Use of the peak flux (2.57 kw/cm^2) in the calculations would lead to significantly greater mass loss rates. However, utilization of the average intensity appears reasonable since the experiments themselves represent a spatially average response to irradiation which includes the effects of non-uniform beam intensity.

Figures 7 and 8 show the computed variation in recession rate V with time for I_0 values of 1.81 and 2.79 kw/cm^2, respectively. The inset curve in each figure indicates the short-time response. Once the sublimation condition is attained at $t = t_0$, an initial rapid increase in V is apparent followed by a significant period during which the irradiated surface advances at a relatively uniform velocity. Figure 7 also indicates that at longer exposure times V again increases somewhat as the moving front surface approaches the back face. This latter effect simply reflects a less severe temperature gradient ahead of the front surface which is caused by the insulation condition imposed at $x = l$. This reduced gradient implies that the second term on the right hand side of Eq. (4) becomes larger (less negative) indicating higher values of V.

The nearly constant recession rate displayed over much of the exposure time may be approximated by consideration of the steady state solution of Eqs. (1-7) for a semi-infinite plate. Regarding V and all material properties as constant and requiring that $T \to T_0$ as $z \to \infty$, the solution is

$$T(z) = (T_s - T_0) \exp\left[\frac{-\rho V C_p z}{k}\right] + T_0,$$

which may be inserted into Eq. (4) to give

$$V = \frac{\alpha I_0 + I_r + I_c}{\rho[H_s + C_p(T_s - T_0)]}.$$

Evaluation of I_r, I_c, and material properties at $T_s = 3316$°C provides the following dependence of V on I_0 for the present experiments:

$$V(\text{mm/sec}) = 0.156\, I_0 - 0.150,$$

where I_0 has units of kw/cm^2. As indicated by the dashed lines in Figs. (7) and (8), this relationship provides a good estimate of the average velocity over the exposure times indicated and may prove useful in projecting plate burnthrough times for AS/3501-6 composite.

Although the numerical treatment presented in this study is adequate for most engineering studies associated with elevated temperature composite behavior, improved modeling is undoubtedly possible. Further examination of the calculated thermal responses shown in Figs. 3-5 indicates that the analysis consistently underestimates the measured interior temperatures and tends to overestimate the rear surface values. Improved correlations at the back surface may result if reduced thermal conductivity values were introduced at low tempeteratures, and Ref. (9) contains experimental conductivity data which would support such an approach. In addition, a recent study (1) of graphite epoxy exposed to flame heating has established that *exothermic* resin decomposition is possible and a kinematic expression quantifying the associated heat generation has been proposed. Inclusion of such a heat source term in the conduction equation should lead to higher predicted temperatures inside the laminate and better agreement with experimental results.

5. SUMMARY

The primary conclusions from the present study of the thermal response of graphite epoxy composite subjected to rapid heating include:

- The proposed one-dimensional numerical model coupled with the material properties contained in Ref. (3) provides temperature distributions and ablative response which are in good agreement with experimental results from laser irradiation tests. When incorporated with appropriate stress computations, the present analysis provides a practical method for projecting the effects of severe thermal environments on composite plate structures.

- The present numerical results indicate that a steady state thermal response is approximately achieved over a significant portion of the exposure times investigated. Analytic expressions for the temperature distribution and recession rate under these conditions have been given.

- Suggestions for improved modeling include incorporation of exothermic matrix decomposition kinetics and the inclusion of reduced bulk thermal conductivity values at low temperature.

REFERENCES

1. G.A. Pering, P.V. Farrell, and G.S. Springer, "Degradation of Tensile and Shear Properties of Composites Exposed to Fire or High Temperature," Journal of Composite Materials, Volume 14, Jan. 1980, p. 54.

2. K.G. Kibler, H.G. Carter, and J.R. Eisenmann," Response of Graphite Composites to Laser Irradiation," TR-77-0706, Air Force Office of Scientific Research (Bolling Air Force Base, DC), March 1977.

3. J.F. Menousek and D.L. Monin, "Laser Thermal Modeling of Graphite Epoxy," NWC Technical Memorandum Report 3834, Naval Weapons Center (China Lake, CA), June 1979.

4. B.A. Baley and J.H. Weiner, *Theory of Thermal Stresses*, John Wiley and Sons, Inc., April 1967, p. 190.

5. H.S. Carslaw and J.C. Jaegar, *Conduction of Heat in Solids*, Oxford Univ. Press, 1959, p. 15.

6. M.I. Cohen, "Melting of a Half-Space Subjected to a Constant Heat Input," Journal of the Franklin Institute, Vol. 283, No. 4, April 1967, p. 271.

7. N.P. Hobbs, T.A. Dalton, and R.F. Smiley, "TRAP2-A Digital Computer Program for Calculating the Response of Mechanically Loaded Structures to Laser Irradiation," KA TR-143 Kamon Avidyne (Burlington, Mass.), October 1977.

8. D.D. McCracken and W.S. Dorn, "Numerical Methods and Fortran Programming," John Wiley and Sons, Inc., 1964, p. 384.

9. J.F. Menousek, R.L. Herring, and E.W. Wiggins, "Thermal Properties of Graphite Epoxy at Elevated Temperatures," MDC-IR0115, McDonnell Aircraft Company (St. Louis, Missouri), Dec. 1978.

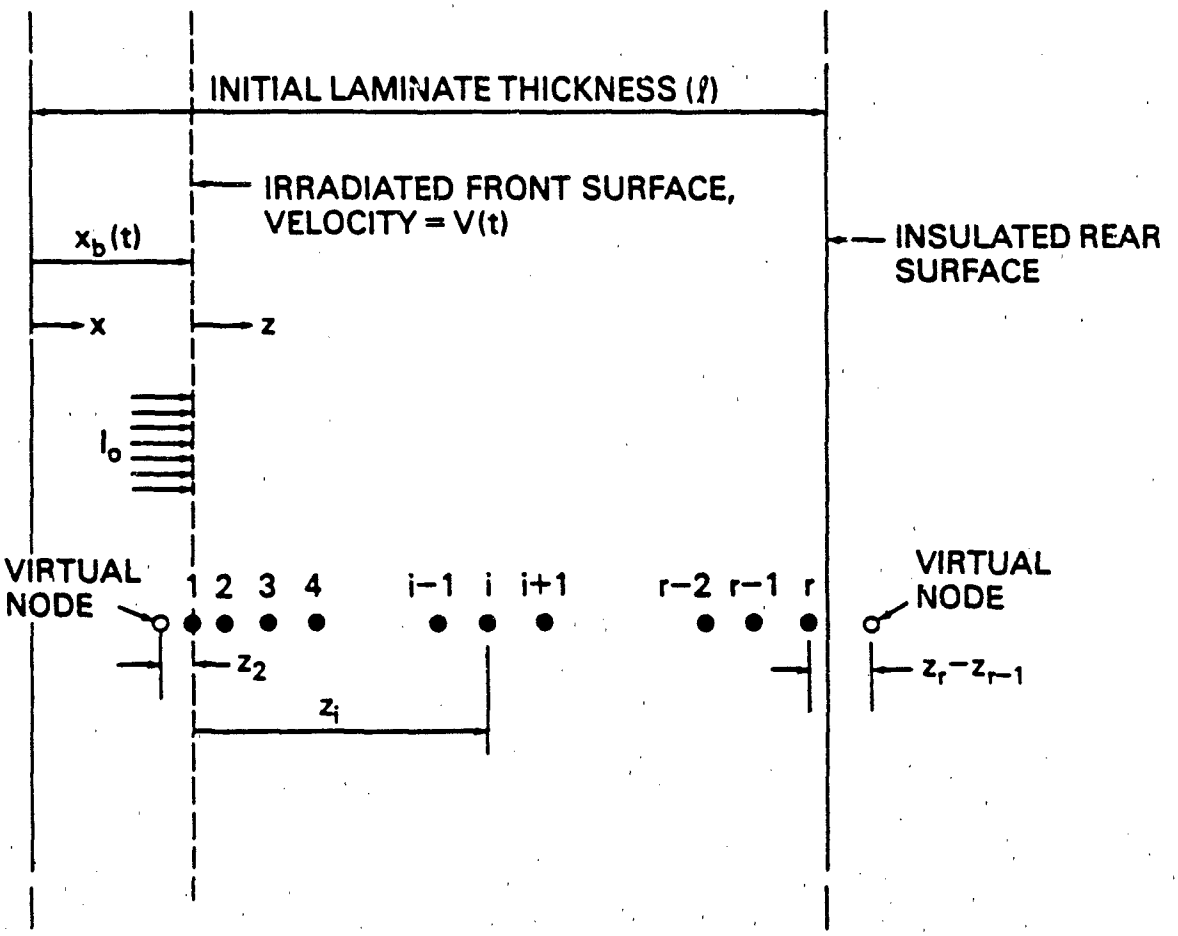

Figure 1 — Convected Coordinate System and Finite Difference Grid Employed in One-Dimensional Analysis.

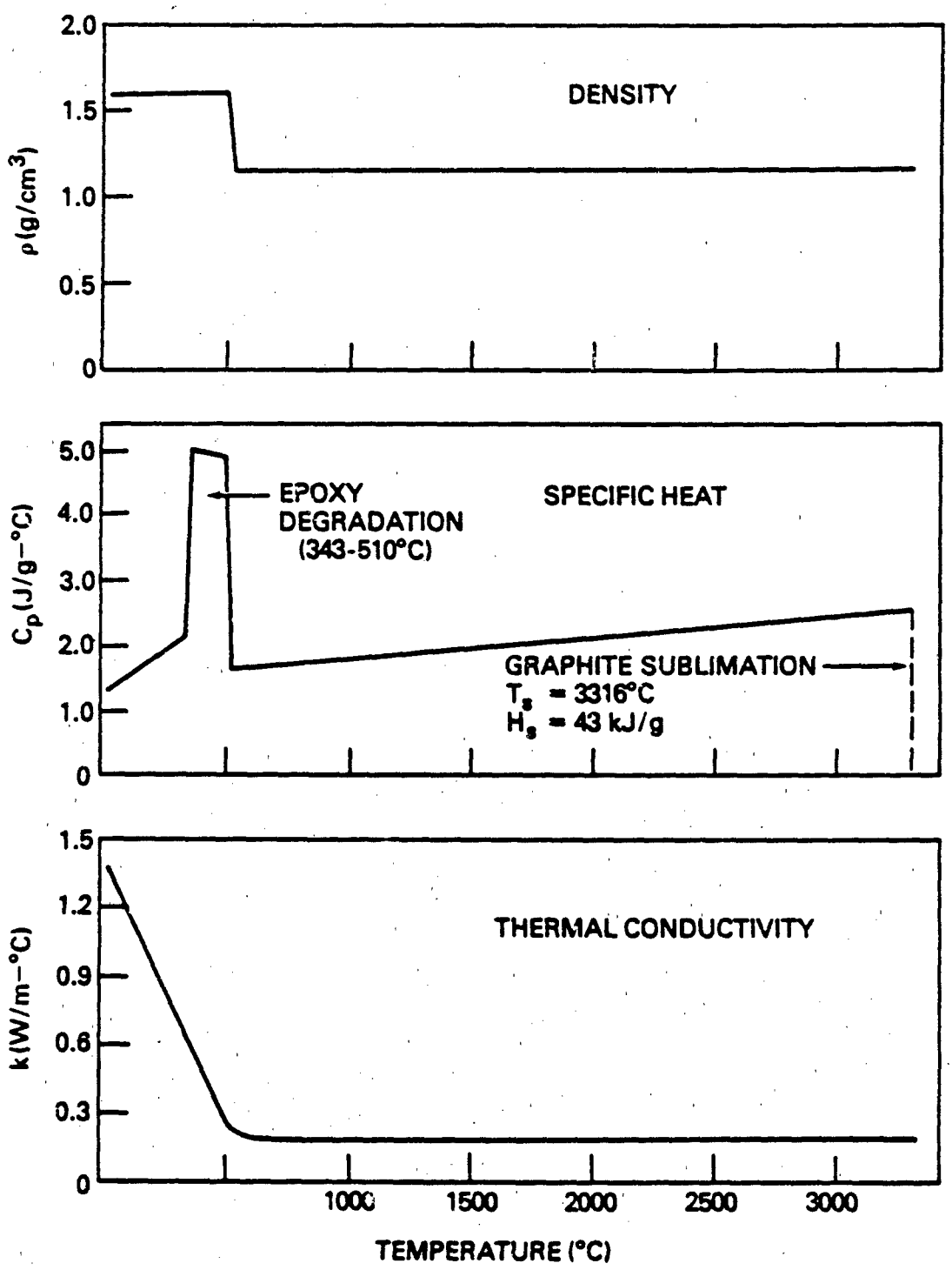

Figure 2 — Temperature Dependence of Thermophysical Properties for AS/3501-6 Composite.

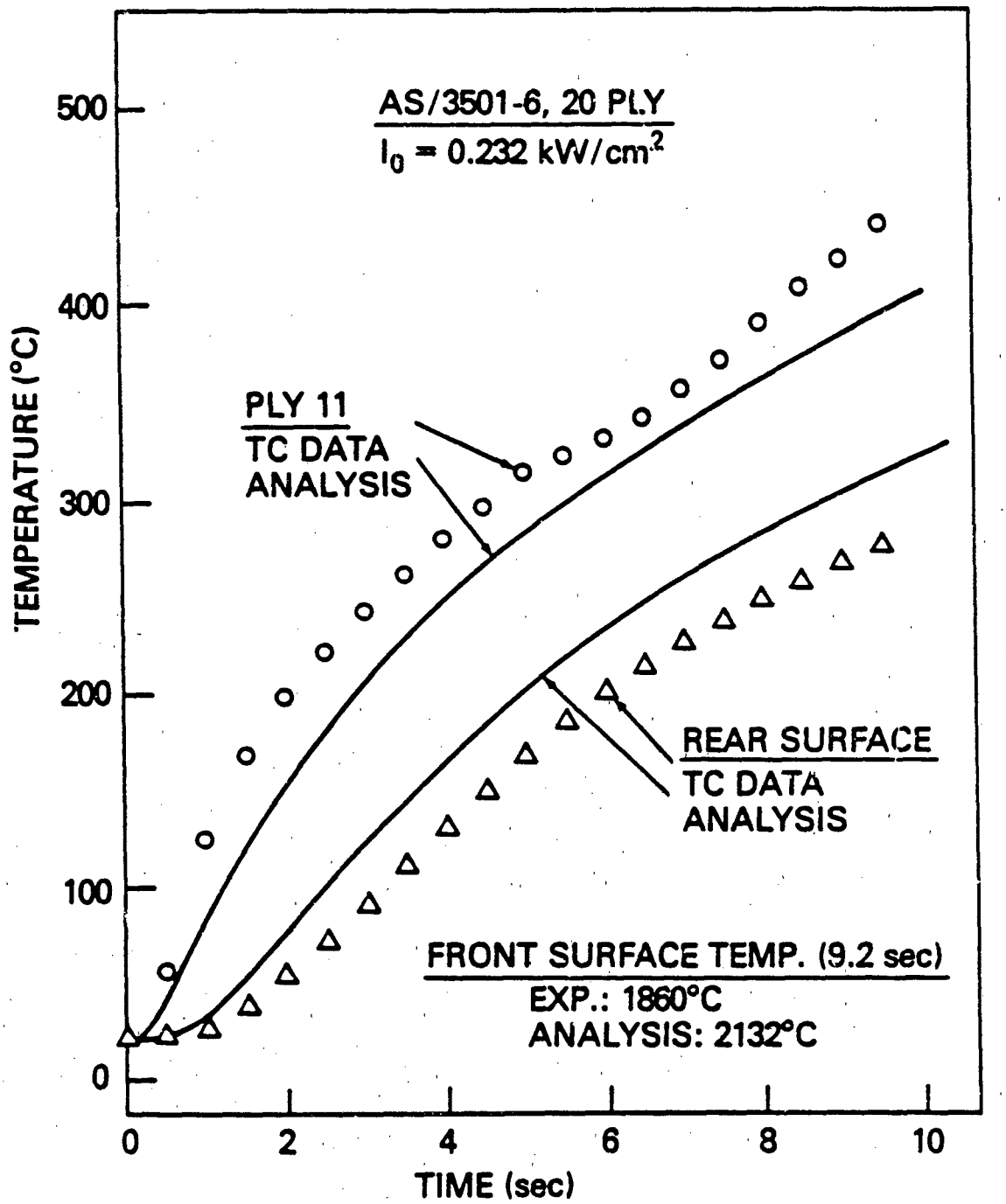

Figure 3 — Comparison of Measured and Predicted Temperature Response for AS/3501-6 Laminate. Beam Intensity = 0.232 kw/cm^2.

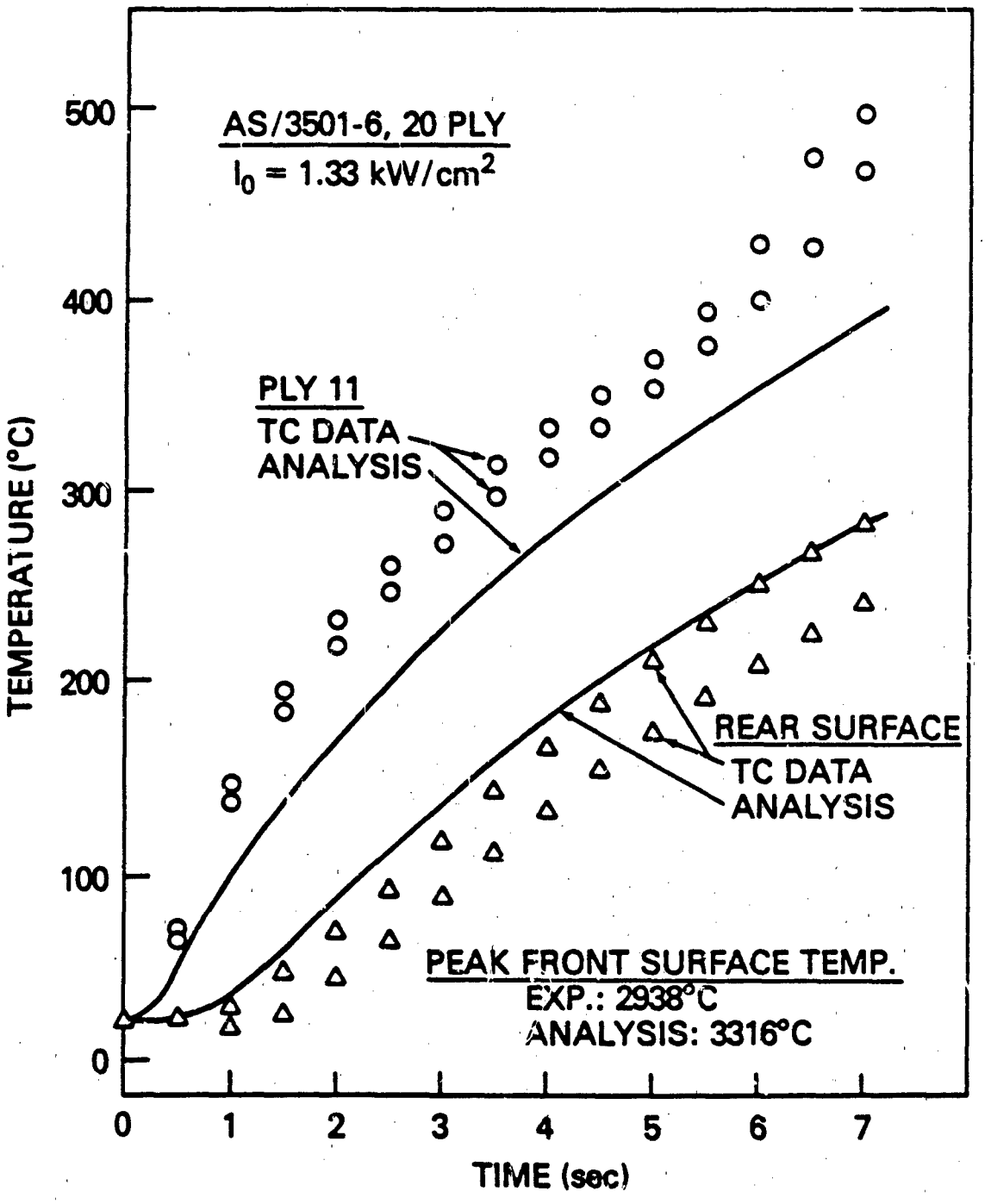

Figure 4 — Comparison of Measured and Predicted Temperature Response for AS/3501-6 Laminate. Beam Intensity = 1.33 kw/cm^2.

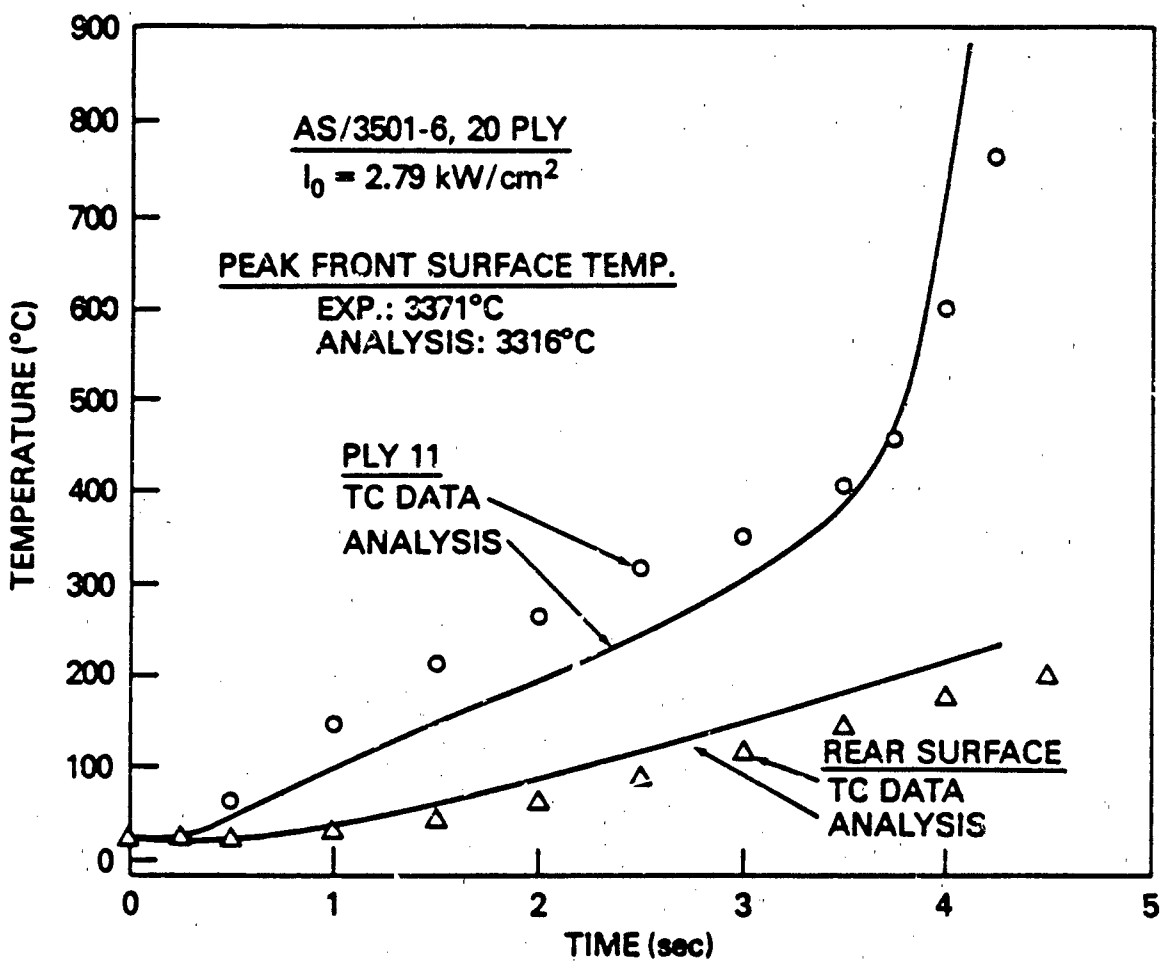

Figure 5 — Comparison of Measured and Predicted Temperature Response for AS/3501-6 Laminate. Beam Intensity = 2.79 kw/cm^2.

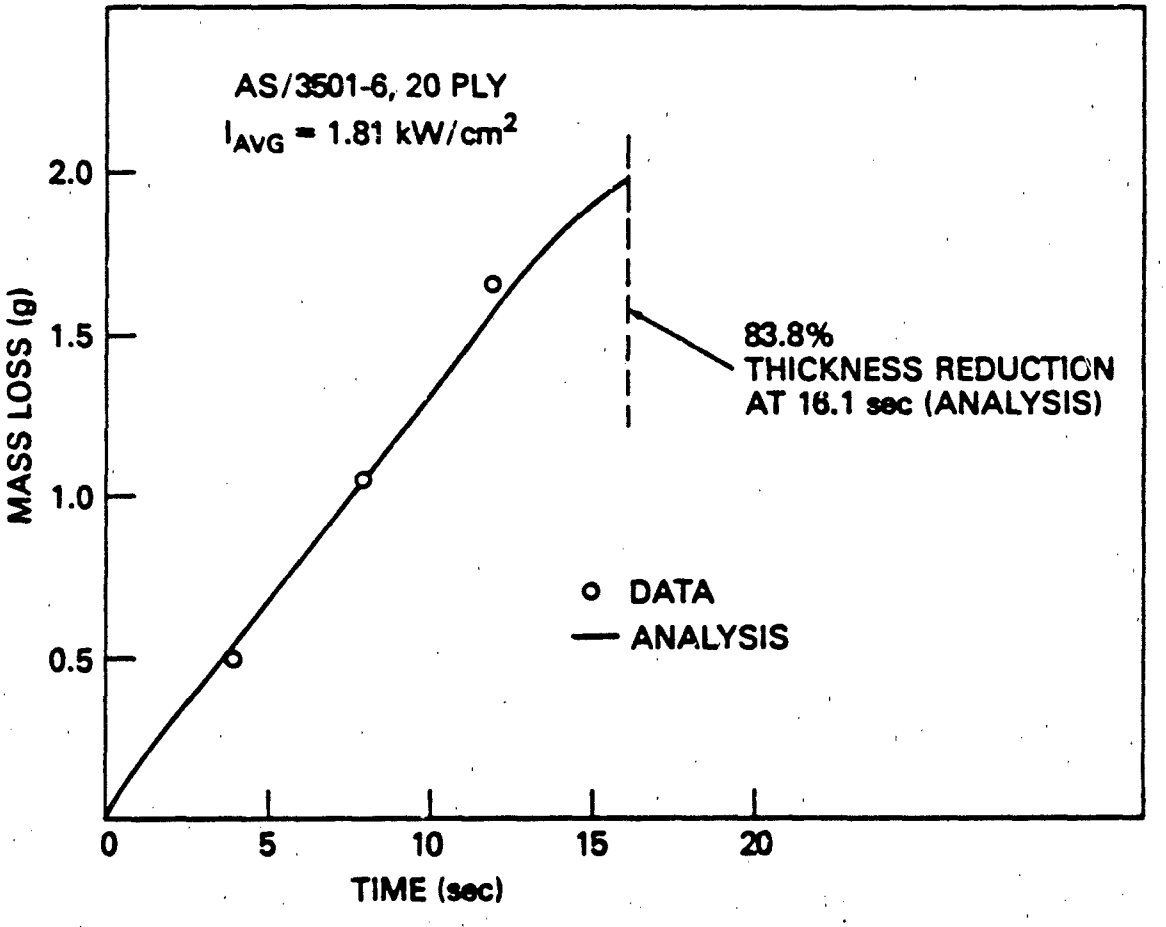

Figure 6 — Experimental and Analytically Derived Mass Loss as a Function of Exposure Time. Average Beam Intensity = 1.81 kw/cm^2.

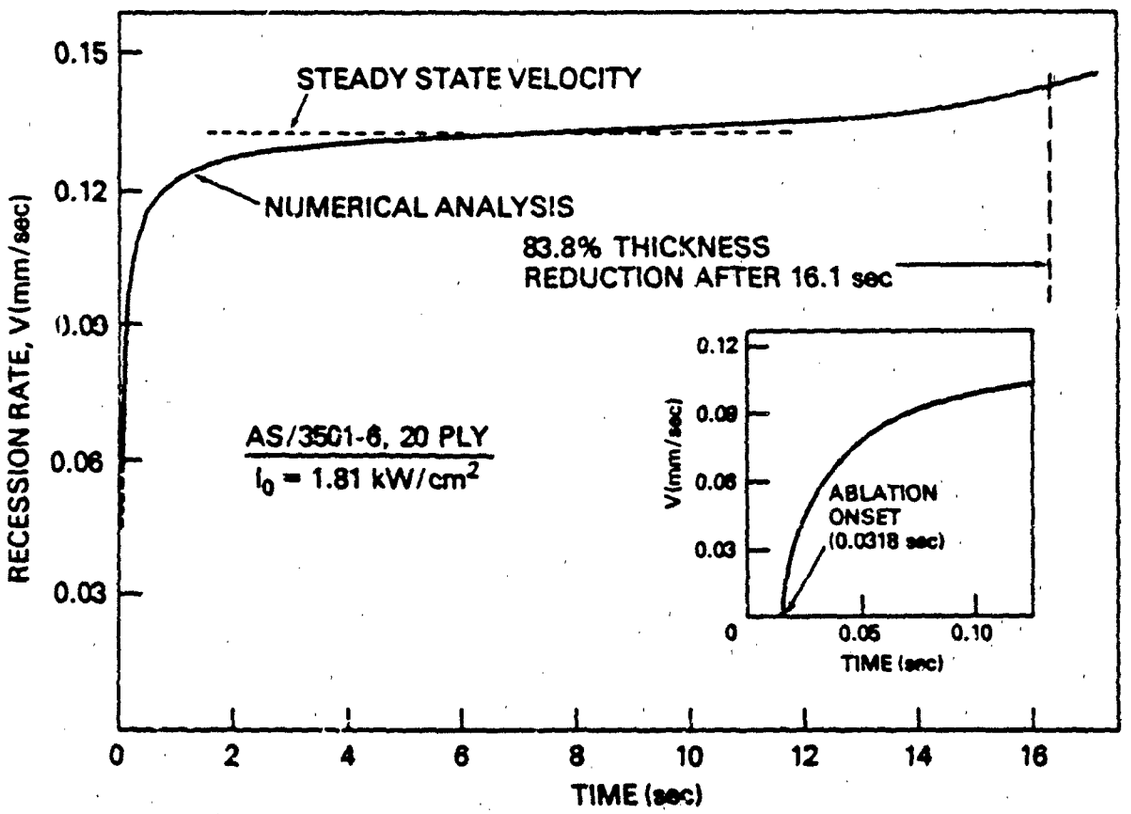

Figure 7 — Variation of Recession Rate with Exposure Time for 1.81 kw/cm^2 Beam Intensity.

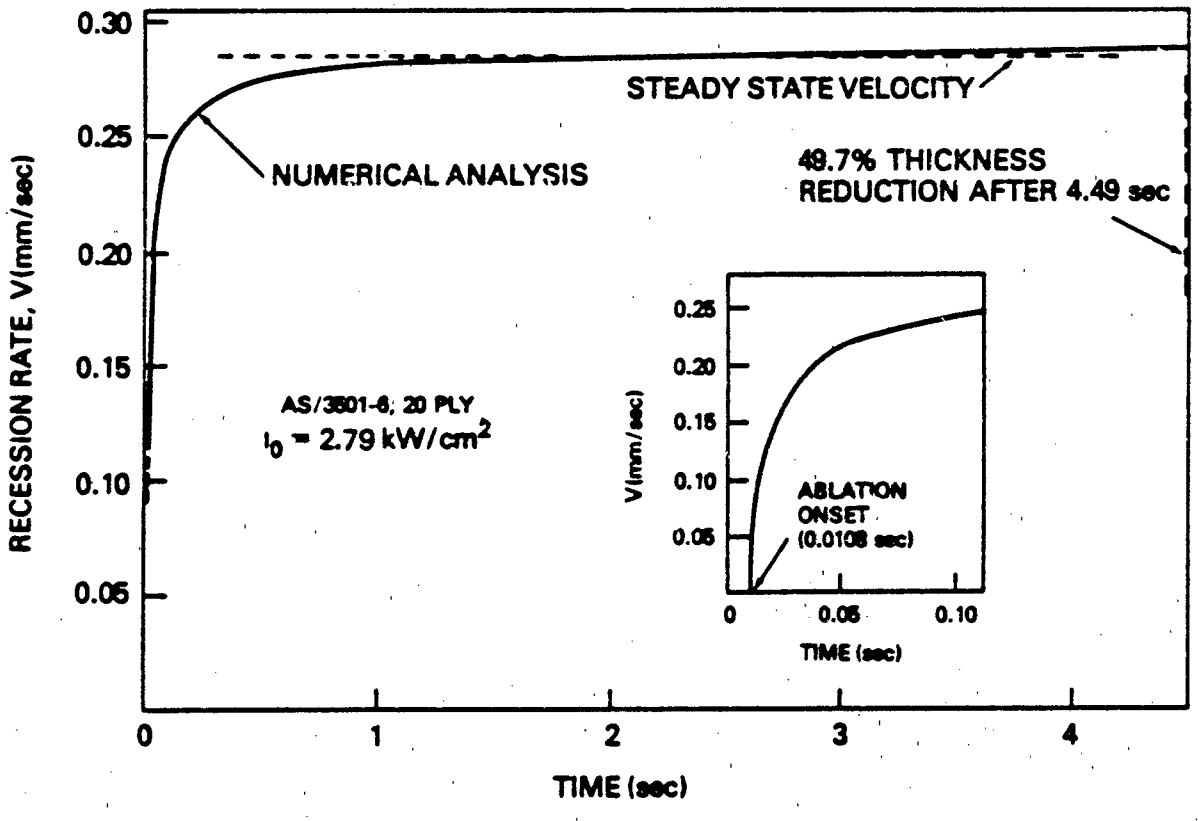

Figure 8 — Variation of Recession Rate with Exposure Time for 2.79 kw/cm^2 Beam Intensity.